BMC Medical Imaging

RESEARCH Open Access

Imaging and clinical manifestations of hematogenous dissemination in melioidosis

Anle Yu[1*†], Lanfang Su[1†], Qun Li[2], Xiaohua Li[1], Sile Tao[3], Feng Li[1] and Danqiong Deng[1]

Abstract

Background Although there is a high incidence of hematogenous infections in melioidosis, a tropical infectious disease, there are few systematic analyses of hematogenous melioidosis in imaging articles. A comprehensive clinical and imaging evaluation of hematogenous melioidosis be conducted in order to achieve early diagnosis of the disease.

Materials and methods We conducted an analysis of 111 cases of melioidosis diagnosed by bacteriological culture between August 2001 and September 2022. The analysis focused on observing the main manifestations of chest imaging and clinical data, including nodules, cavities, consolidation, ground glass opacity(GGO), pleural effusion, centrilobular nodules, and temperature, leucocyte count, diabetes, etc. Our study involved univariate and multivariate analyses to identify significant diagnostic variables and risk predictive factors.

Results A total of 71.2% (79/111) of melioidosis cases were caused by hematogenous infection, and the most common organ involved was the lungs (88.5%, 100/113). The incidence of sepsis in patients with lung abnormalities was high (73%, 73/100), and the mortality rate of septic shock was 22% (22/100). Univariate analysis showed that the radiologic signs of blood culture-positive cases were more likely to have bilateral pulmonary and subpleural nodules ($p=0.003$), bilateral GGO ($p=0.001$), bilateral hydrothorax ($p=0.011$). The multivariate analysis revealed a significant improvement in the area under the receiver operating characteristic curve (AUC) when comparing the model that included both clinical and radiologic variables to the model with clinical variables alone. The AUC increased from 0.818 to 0.932 ($p=0.012$). The most important variables in the logistic regression with backward elimination were found to be nodule, GGO, and diabetes.

Conclusion The combination of CT features and clinical variables provided a valuable and timely warning for blood borne infectious melioidosis.

Keywords Diagnostic imaging, Melioidosis, Burkholderia pseudomallei, Bacteremia, Early diagnosis

†Anle Yu and Lanfang Su are co-first authors who made equal contributions to this study.

*Correspondence:
Anle Yu
yallq2004@163.com

[1]Department of Radiology, The First Affiliated Hospital of Hainan Medical University, 31 Longhua Rd, Haikou, Hainan, China
[2]Department of Pathology, The First Affiliated Hospital of Hainan Medical University, 31 Longhua Rd, Haikou, Hainan, China
[3]Department of Data Science, Quartic.ai, 1050 King St W, Toronto, ON, Canada

Background

Melioidosis, caused by the environmental gram-negative bacillus Burkholderia pseudomallei, is an infectious disease primarily found in tropical regions [1, 2]. Burkholderia pseudomallei is predominantly prevalent in northern Australia and Southeast Asia [2–4]. Melioidosis has a high incidence of bacteremia, ranging from 40 to 69% [5–8]. This bacteremia can result in septic shock necessitating intensive care, mechanical ventilation, or renal dialysis treatment, and is associated with a high mortality rate [7–10]. In resource-limited areas, the mortality rate of melioidosis can reach as high as 50–70% [1, 2, 5, 11].

In clinical practice, pneumonia is the predominant manifestation of melioidosis, accounting for over 50% of cases [7–12]. Additionally, multiple abscesses in the liver and spleen were observed as another significant presentation [12, 13]. Pulmonary infections caused by bacteremia are highly prevalent in patients with melioidosis, with incidence rates reaching up to 62% [7]. However, melioidosis is a neglected cause of community-acquired pneumonia [1, 2, 11].

Melioidosis exhibits diverse and complex clinical manifestations in addition fever, often resembling various diseases, earning it the reputation of being a 'great mimicker' [1, 2, 14]. Diagnosing melioidosis based solely on clinical grounds is highly challenging due to its nonspecific clinical presentation [1, 3, 4, 8]. Compared with clinical reports, imaging descriptions of melioidosis in publications tend to receive less attention. While the imaging manifestations of hematogenous melioidosis are primarily reported on X-ray chest films, some articles have also described CT findings in the lungs, abdomen, and other organs [9–13, 15–20]. However, few studies have systematically analyzed and evaluated the CT manifestations of hematogenous melioidosis in the lungs and other organs.

Early detection of bloodstream infections can prompt a rapid clinical response and is crucial for controlling sepsis and septic shock. This article presents a retrospective analysis of the imaging and clinical features of bloodborne infectious melioidosis in order to facilitate early diagnosis and treatment.

Materials and methods

This study was approved by the Ethics Committee of The First Affiliated Hospital of Hainan Medical University and the requirement for informed consent was waived.

We identified 114 cases of melioidosis diagnosed by bacteriological culture between August 2001 and September 2022. Three patients with positive bacteriological cultures but no imaging data were excluded, while 111 patients with both bacteriological culture diagnosis and imaging were enrolled. 79 cases with positive blood cultures were included in the blood culture-positive group, of which 19 cases also showed positive cultures for pus, sputum, or pleural effusion. 32 cases who were confirmed positive by other body fluids (secretions) were classified into the blood culture-negative group.

In the other two cases suffering from type 2 diabetes mellitus, no pathogenic bacteria were found in the bacteriological culture through various ways. Clinical evaluations, along with pulmonary and extrapulmonary imaging, collectively demonstrated the presence of sepsis. The patient's symptoms did not improve after treatment with multiple antibiotics. Empirical therapy for melioidosis was effective, resulting in the symptoms improved. Most lung and extrapulmonary lesions were absorbed and the patient was discharged from the hospital after imaging reexamination. These two cases were included in the blood culture-negative group, resulting in 34 cases in the blood culture-negative group. The total number of patients in this group was 113.

All clinical features and risk factors are shown in Table 1.

The types of chest imaging data for the 113 cases were as follows: 89 chest CT data, 24 chest X-ray data, among the 113 cases 17 having both chest CT and chest X-ray data. Among the 113 cases, 64 showed the involvement of extrapulmonary organs and corresponding imaging examinations. Some patients present with multiple organ (site) involvement.

Chest CT scanning parameters were(1) axial, slice thickness, 5 mm, space, 5 mm; (2) lung window: window width, 1600HU, central, -600HU; and (3) mediastinal window: window width, 350HU, central, 50HU.

Imaging observation content

Chest and body imaging

(1) Chest imaging findings, it can be divided into two categories: with and without lung abnormalities. The main image findings include nodules, subpleural micronodules that refer to the nodules with a diameter < 6 mm are in the subpleural region, and accompanying peribronchovascular interstitium and interlobular septal thickening [21], cavities, consolidation, ground glass opacity (GGO), intra- and interlobular septal thickening, pleural effusion, and centrilobular nodules (tree-in-bud sign). The above imaging findings represent lung abnormalities. In this article, GGO specifically refers to the hazy increased opacity of the lung on a conventional 5 mm slice CT film, where pulmonary blood vessels can be seen, and some can show intra- and interlobular septal thickening.

(2) Patients with chest imaging manifestations were divided into two groups based on the location of the lesion: unilateral lung distribution and bilateral lung distribution.

(3) Mediastinal lymph node enlargement was divided into two groups: with and without lymph node

Table 1 Association of blood culture with clinical features

Variable	All cases ($n=113^{\oint}$)	No. of blood culture		*P*-Value*	Univariate OR†
		Negative	Positive		
Sex					
Male	102	30	72	0.731	Reference
Female	11	4	7		0.729 (0.199, 2.676)
Median age	53 (1, 81)	54 (1,73)	53 (1,81)	0.978	1.004 (0.978, 1.031)
Temperature					
Temperature < 39 ℃	10	10	0	0.000	Reference
Temperature ≥ 39 ℃	103	24	79		0.999 (0.000, NAN)
Leukocyte					
Leukocyte < 10^9/ L	40	11	29	0.830	Reference
Leukocyte ≥ 10^9/ L	73	23	50		0.825 (0.352, 1.933)
diabetes					
No	40	19	21	0.005	Reference
Yes	73	23	50		3.498 (1.509, 8.112)
Alcoholic					
No	89	30	59	0.135	Reference
Yes	24	4	20		2.542 (0.797, 8.110)
Malignancy‡					
No	108	34	74	0.320	Reference
Yes	5	0	5		0.999 (0.000, NAN)
Smoking					
No	56	18	38	0.637	Reference
Yes	57	16	41		1.214 (0.543, 2.715)

Note OR = odds ratio. NA = Not applicable. NAN = not a number

$\oint$ Two clinically confirmed cases were classified as blood culture negative group

* P-value was computed by comparing the blood culture positive group with the negative group

† Data in parentheses are 95% confidence intervals

‡ There were 5 patients with malignancy, including 1 lung cancer, 1 nasopharyngeal carcinoma, 1 esophageal cancer, 1 liver cancer, and 1 acute lymphocytic leukemia

enlargement. Lymphadenopathy is defined as a short-axis CT measurement of lymph nodes ≥ 10 mm [22].

(4) Lesions in other organ sites of the body, combined with the presence or absence of lung lesions, were divided into two groups: those with and without lung lesions.

Observation data acquisition

Two experienced radiologists, both blinded to the bacteriological examination results, independently evaluated the imaging manifestations in the lungs. One radiologist (L S) had 14 years of experience in imaging diagnosis, while the other (D D) had 26 years of experience in the field. In cases where there were inconsistent observation results, a third senior physician (A Y) with 40 years of experience in chest imaging diagnosis, who was also blinded to the previous observations, was consulted. The results were determined based on the consensus of two out of the three viewers. Clinical data was collected from medical records by one physician and independently reviewed by another physician.

Statistical analysis

The main statistical analyses were performed by using IBM SPSS Statistics (version 26). Python (version 3.9) was utilized to generate receiver operating characteristic (ROC) curves, and DeLong test [23] was performed using the open source Python package roc_comparison [24].In the analysis of the association between blood culture and imaging and clinical features, the Wilcoxon rank-sum test was used to compare age medians between different bloodstream infection status, given the non-normal distribution of the data. Fisher's exact test was used for binary categorical variables to ensure reliable P-values with small cell counts. For categorical variables with more than two levels, the chi-square test was used. Logistic regression was performed to identify independent factors that can be used to predict blood-borne infection. The areas under the receiver operating characteristic curve (AUC) of two models were compared using the nonparametric DeLong test, and a two-sided P-value < 0.05 indicated a significant difference. The final logistic regression model was selected with a backward elimination method, using a p-removal threshold of 0.10.

Cohen's Kappa was conducted to assess interobserver consistency for various lung and extrapulmonary imaging manifestations.

Results

Consistency of lung and extrapulmonary imaging evaluation results

The results obtained by the two observers for various lung and extrapulmonary abnormalities were consistent (Table 2).

Bacteria culture

Among the 113 patients in this group, 111 were confirmed to be infected with Burkholderia pseudomallei by laboratory bacterial culture. Among these, 79 cases (71.2%) were confirmed by blood culture and classified as blood culture positive. 32 cases (28.8%) were confirmed

Table 2 Statistical consistency of observation results between two imaging experts

CT Feature	Kappa value	*P*
Nodule	0.926	<0.001
Cavety	0.968	<0.001
Consolidation	0.937	<0.001
GGO	0.864	<0.001
Hydrothorax	0.925	<0.001
Lymphadenopathy	0.942	<0.001
Centrilobular nodules	0.812	<0.001
Extrapulmonary lesions	1.000	<0.001

by other body fluid or secretion cultures and were classified as the blood culture-negative group. Other cultures included sputum (5 patients, 4.5%), pus (15 patients, 13.5%), urine (3 patients, 2.7%), tracheal and alveolar lavage fluid (3 patients, 2.7%), puncture fluid (5 patients, 4.5%), and peritoneal dialysis fluid (1 patient, 0.9%). Another 2 cases were confirmed by clinical diagnostic therapy, with 34 cases in the negative group.

The average time for obtaining bacteriological culture results was 4 days (1–9 days).

Association of hematogenous infection with clinical features

113 patients were included in this study. Associations between blood culture with clinical features are presented in Table 1. Two clinical features were found to be associated with hematogenous infection: temperature is ≥39 °C (P=0.000) and the presence of diabetes (P=0.005).

Association of hematogenous infection with radiologic features

Univariate analysis revealed that 3 radiologic features were associated with hematogenous infection, including nodule (P=0.003), GGO (P=0.001) and hydrothorax (P=0.011). Compared to the reference groups, bilateral nodules (OR, 4.911; 95% CI: 1.904, 12.665), bilateral GGO (OR, 4.800; 95% CI: 1.637, 14.073), bilateral hydrothorax (OR, 7.176; 95% CI: 1.975, 26.075) were more prevalent in the blood culture positive group than the Blood culture negative group (Table 3).

The kind of nodules in both lungs varies in morphology on imaging, with most of them being solid nodules and a small amount being partial solid nodules and ground glass nodules observed at a thickness of 5 mm on CT (Figs. 1 and 2).

Among the 113 patients, 100(88.5%, 100/113) had lung abnormalities. There were 29 cases of septic shock (25.7%, 29/113), of which 28 cases were in the group of pulmonary abnormalities (28%, 28/100). 23 deaths in this study, among them 22 deaths in the lung abnormality group, of which 21 cases were positive for blood culture, and the remaining one patient died in the normal lung group, and the blood culture was positive [Electronic Supplementary Material (ESM) Table 1].

There were 64 cases of extrapulmonary lesions within the 113 cases of the study. Most cases were found in those with a positive blood culture accompanied by pulmonary abnormalities (78.2%, 43/55; ESM Table 1, ESM Fig. 1), and the positive rate of blood culture in the group with extrapulmonary lesions accompanied by pulmonary abnormalities was higher than that in the group with extrapulmonary lesions without pulmonary abnormalities (11.1%, 1/9; ESM Table 1). However, based on blood culture results, the proportion of extrapulmonary lesions in cases with positive and negative blood cultures was similar (57.7% vs. 58.8%, Table 1).

In the bilateral lung GGO group with positive blood culture, five cases showed appearance of resembling irregularly shaped paving stones (indicative of intra-lobular septal thickening) and four cases showed thickening of the interlobular septa (Figs. 3, 4 and 5,). In the negative blood culture group, three cases showed thickening of the interlobular septa, one of them with the lesion limited to the right upper lobe, GGO and thickening of the interlobular septa were visible, and a right hilar mass accompanied by mediastinal lymph node enlargement was misdiagnosed as lung cancer. No malignant cells were found on the lymph node biopsy, and the culture of the alveolar lavage fluid was positive for Burkholderia pseudomallei.

Multivariate analysis of prognostic factors and ROC curve analysis

Logistic regression analyses were performed using only clinical variables and both clinical and radiologic variables (Tables 4 and 5). When comparing the model including both clinical and radiologic variables to the model with clinical variables alone, the AUC increased from 0.818 to 0.932 (P=0.012, Fig. 6; Table 6). The most important variables in the logistic regression with backward elimination (ESM Table 2) were found to be nodule, GGO, and diabetes.

Involvement of extrapulmonary organs

The number of extrapulmonary organs involved was on average one, with as many as four. The most frequently involved organs outside the lung were the liver and spleen (39.1%, 25/64;ESM Table 1).

Discussion

The investigation of imaging and clinical findings showed that bilateral intrapulmonary and subpleural nodules, bilateral intrapulmonary GGO, and diabetes were independent risk factors for hematogenous melioidosis. When comparing the model that includes clinical and

Table 3 Association of blood culture with radiologic features

Variable	Patients ($n=113^{\oint}$)	No. of blood culture		*P* Value*	Univariate OR†
		Negative	Positive		
Nodule				0.003	NA
No nodules	35	17	18	NA	Reference
Unilateral nodules	16	7	9	0.749	1.214 (0.370, 3.990)
Bilateral nodules	62	10	52	0.001	4.911 (1.904, 12.665)
Cavity				0.875	NA
No cavities	66	20	46	NA	Reference
Unilateral cavites	31	10	21	0.846	0.913 (0.365, 2.286)
Bilateral cavities	16	4	12	0.676	1.304 (0.375, 4.541)
Consolidation				0.082	NA
No consolidation	67	21	46	NA	Reference
Unilateral consolidations	26	11	15	0.320	0.623 (0.245, 1.584)
Bilateral consolidations	20	2	18	0.074	4.109 (0.873, 19.346)
GGO‡				0.001	NA
No GGO	56	21	35	NA	Reference
Unilateral GGO	12	8	4	0.073	0.300 (0.080, 1.119)
Bilateral GGO	45	5	40	0.004	4.800 (1.637, 14.073)
Hydrothorax				0.011	NA
No hydrothorax	61	25	36	NA	Reference
Unilateral hydrothorax	18	6	12	0.560	1.389 (0.460, 4.193)
Bilateral hydrothorax	34	3	31	0.003	7.176 (1.975, 26.075)
Lymphadenopathy					
No	91	26	65	0.605	Reference
Yes	22	8	14		0.700 (0.263, 1.866)
Centrilobular nodules					
No	78	23	55	0.828	Reference
Bilateral&	35	11	24		0.912 (0.385, 2.164)
Extrapulmonary lesions					
No	49	14	35	0.837	Reference
Yes	64	20	44		0.880 (0.390, 1.987)

Note OR=odds ratio. NA=Not applicable

∮ Two clinically confirmed cases were classified as blood culture negative group

** P-value was computed by comparing the blood culture positive group with the negative group*

† Data in parentheses are 95% confidence intervals. ‡ GGO=Ground glass opacity

& Bilateral lungs distribution of centrilobular nodules and no unilateral lung distribution of them

radiological variables with the model that only includes clinical variables, the area under the receiver operating characteristic curve increased from 0.818 to 0.932 ($P=0.012$, Table 6). Prove that the combination of imaging and clinical indicators is more effective than using clinical indicators alone to predict blood born infectious melioidosis. The research results of Suputtamongkol et al. show that in areas of endemic melioidosis, diabetics were at higher risk of developing melioidosis, especially septicemic disease, than septicemia caused by other bacteria [6]. Our results also confirm that diabetes is an independent high risk factor for hematogenous melioidosis, but failed to collect clinical and imaging data from patients with bacteremia caused by other bacteria for comparison, and that would be helpful for differential diagnosis.

Bilateral pulmonary and subpleural nodules are classic imaging manifestations of various lesions that spread through the blood to the lungs and are the most common imaging manifestations. The pulmonary nodules of melioidosis are larger than those of miliary pulmonary tuberculosis, and both solid and sub-solid nodules can be seen in the lungs, which is different from hematogenous disseminated pulmonary tuberculosis [25]. Nevertheless, it is difficult to distinguish between hematogenous disseminated lesions caused by other pathogens, such as Staphylococcus aureus, Klebsiella pneumoniae etc. [26]. Notably, bilateral subpleural micronodules are easily overlooked [21], which can be observed in some cases of acute hematogenous dissemination in the current study, and the condition develops rapidly. In clinical pratice, risk factors for melioidosis include diabetes, which is the most frequent, heavy alcohol use, genitourinary disease, cancer, etc., and the latter is less common [2–6]. Melioidosis is often misdiagnosed as tuberculosis,

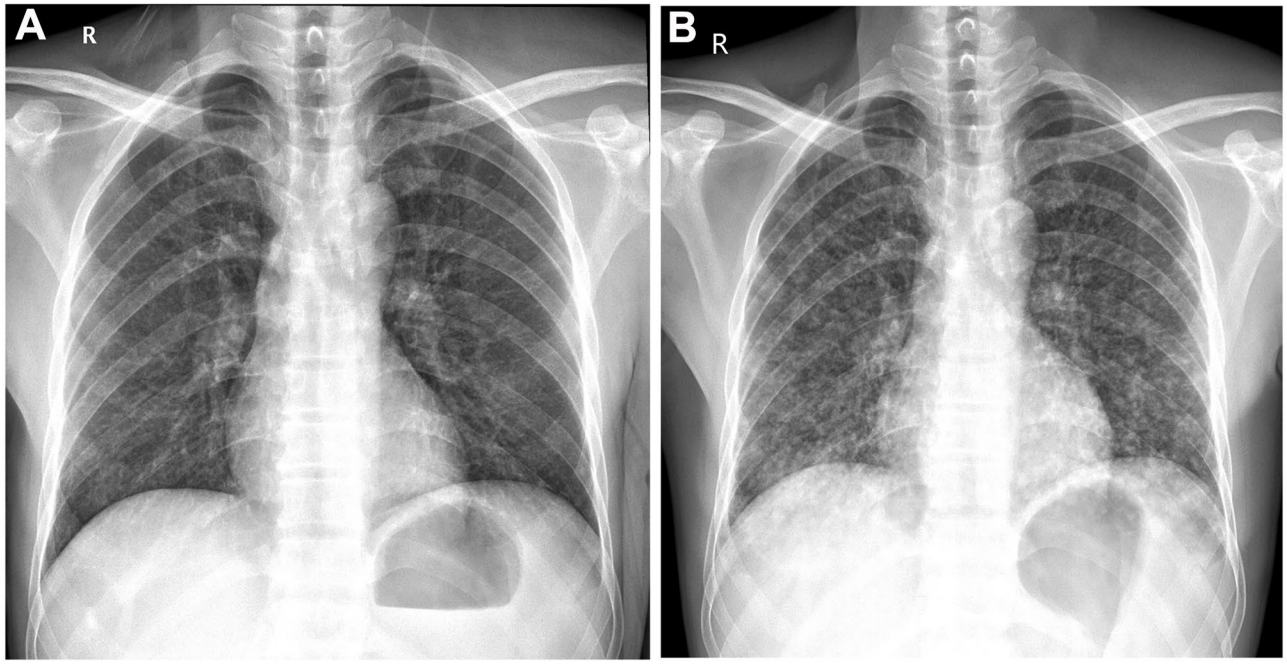

Fig. 1 Plain CT examination obtained in a man with positive blood culture for Burkholderia pseudomallei, being septic shock accompanied by suppurative infection of the left shoulder soft tissue. (**A**) The chest radiography shows an increase in bilateral lung markings, and a reticular shadow faintly displayed in the right lower lung. (**B**) A day later, a chest X-ray was taken and both lungs were covered with nodules, typical manifestation of hematogenous infection. Due to worsening of the condition and ineffective treatment, the patient died

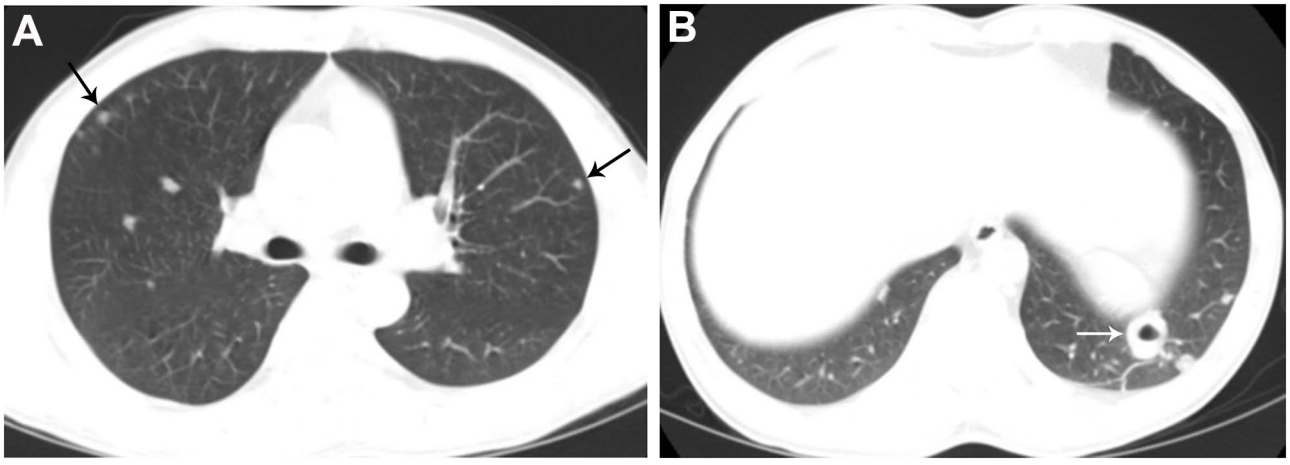

Fig. 2 Plain CT examination obtained in a man with delayed positive blood culture for Burkholderia pseudomallei. (**A**)There are a few nodules in both lungs and sub-pleuras (arrow). (**B**) A cavity formed in a nodule of necrosis and liquefaction at the lower lobe of the left lung(arrow). The patient sustained unexplained high fever with a body temperature of 40.2 ° C, and died after ineffective treatment. The blood culture results were obtained three days after the patient died

community-acquired pneumonia, and sometimes as lung cancer, metastatic tumors, and other diseases in our clinical practice. Due to the non-specific clinical and imaging manifestations of melioidosis, it becomes important to consider the patient's history of living or traveling in endemic areas, and the comprehensive evaluation of clinical findings and laboratory test results, as well as imaging features, especially in the differential diagnosis of blood-borne infectious cases.

In this article, pulmonary GGO in many patients, and the intra-lobular reticulum thickening (crazy-paving pattern) which has not been reported in the literature on melioidosis, and interlobular septal thickening in a small patients can be seen with hematogenous melioidosis.

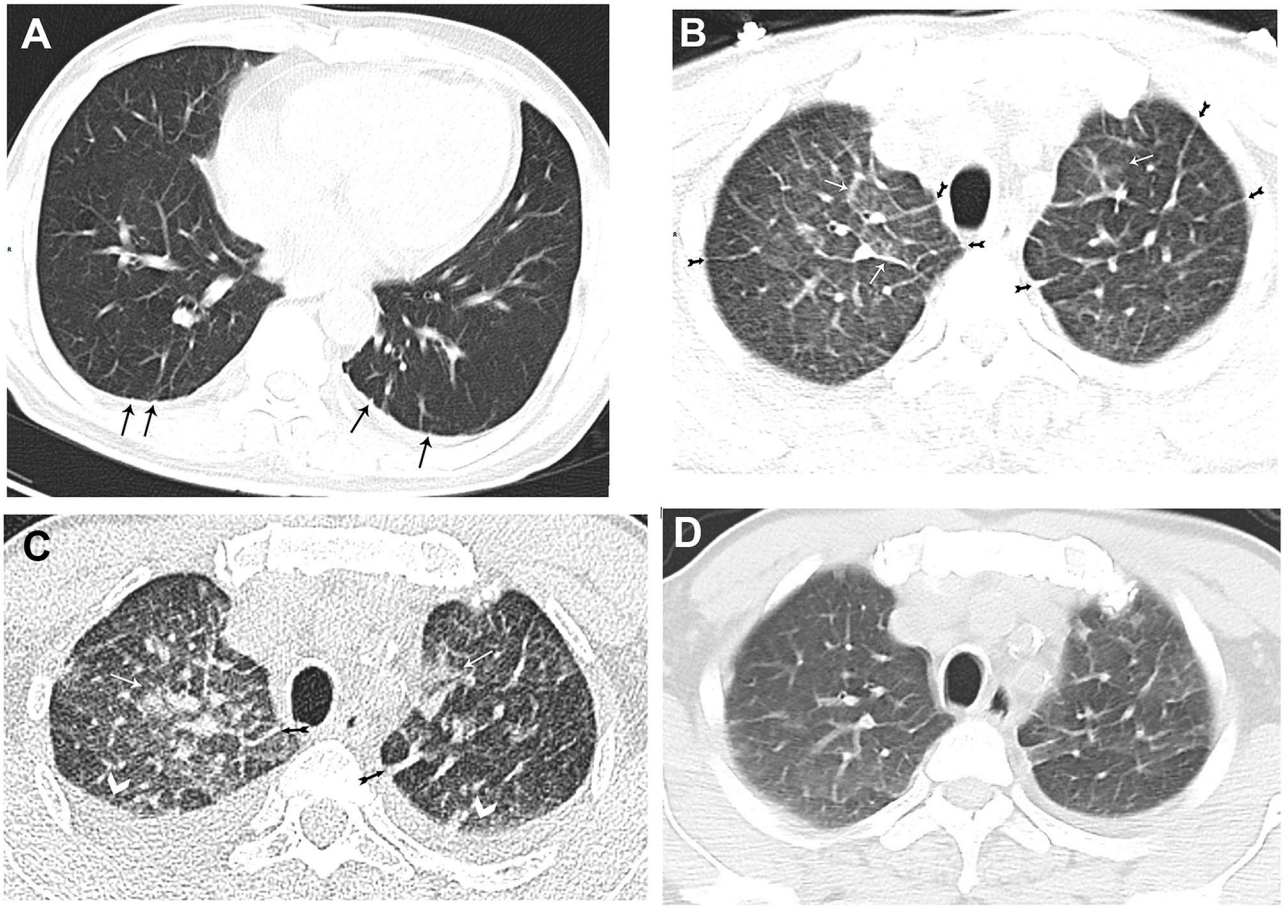

Fig. 3 Plain CT examination obtained in a man with positive blood culture for Burkholderia pseudomallei. Slice thickness of 5 mm (**A**, **B**); Slice thickness of 0.75 mm (**C**). (**A**) A small amount of pleural effusion on both sides. The pleural surface is rough, with a small amount of subpleural micronodules and peribronchovascular interstitium thickening visible (arrow). (**B**) 2 days later reexamination, bilateral intrapulmonary GGO was observed, with lobular GGO in the bilateral upper lobe (white arrow) and thickening of the interlobular septum of both lungs (fish tailed arrow). (**C**) Reexamination in 3 days with thin-section images showed increased pleural effusion on both sides(arrowhead), thickening of interlobular septa(fish tailed arrow), and expansion of ground-glass opacities(white arrow). (**D**) The pulmonary lesions were obviously absorbed after 13 days of treatment

These findings are consistent with those reported by McGuinness et al. for the lungs of patients with hematogenous disseminated diseases [27–29]. Based on the improved absorption after treatment, the authors speculated that the GGO and thickening of the intra- and interlobular septa in the lungs reflect few acute exudative reactions within the alveoli and pulmonary interstitium. Currie et al. [7] reported that the incidence of pneumonia and bacteremia in patients with melioidosis was 52% and 56%, respectively; the incidence of bacteremia in patients with pneumonia was 62%, septic shock was 30%, and the death was 16%. In the study the incidence of pulmonary abnormalities and bacteremia in patients with melioidosis were 88.5% and 69.9%, respectively. The incidence of bacteremia in patients with pulmonary abnormalities was 75%, septic shock was 28.9%, and the death was 22%. The high detection rate of pulmonary lesions in this melioidosis study may be related to the application of CT in lung examinations. CT is superior to chest radiography in displaying GGO, micro- and small nodules, and small amounts of pleural effusion [9, 17, 18, 30]. However, in the early stages of hematogenous melioidosis, such lesions are not easily visible on chest radiography.

The number of cases with bilateral pleural effusion is lower compared to cases with bilateral lung nodules and GGO. Most of these cases are a result of infection spreading to the pleura through the bloodstream [28, 31]. In clinical practice, multiple-organ (site) infections often result from hematogenous dissemination [32, 33]. This study revealed that the positive rate of blood cultures in the group with extrapulmonary lesions and pulmonary abnormalities (78.2%) was significantly higher than that in the group with extrapulmonary lesions without pulmonary abnormalities (11.1%). Although imaging diagnosis

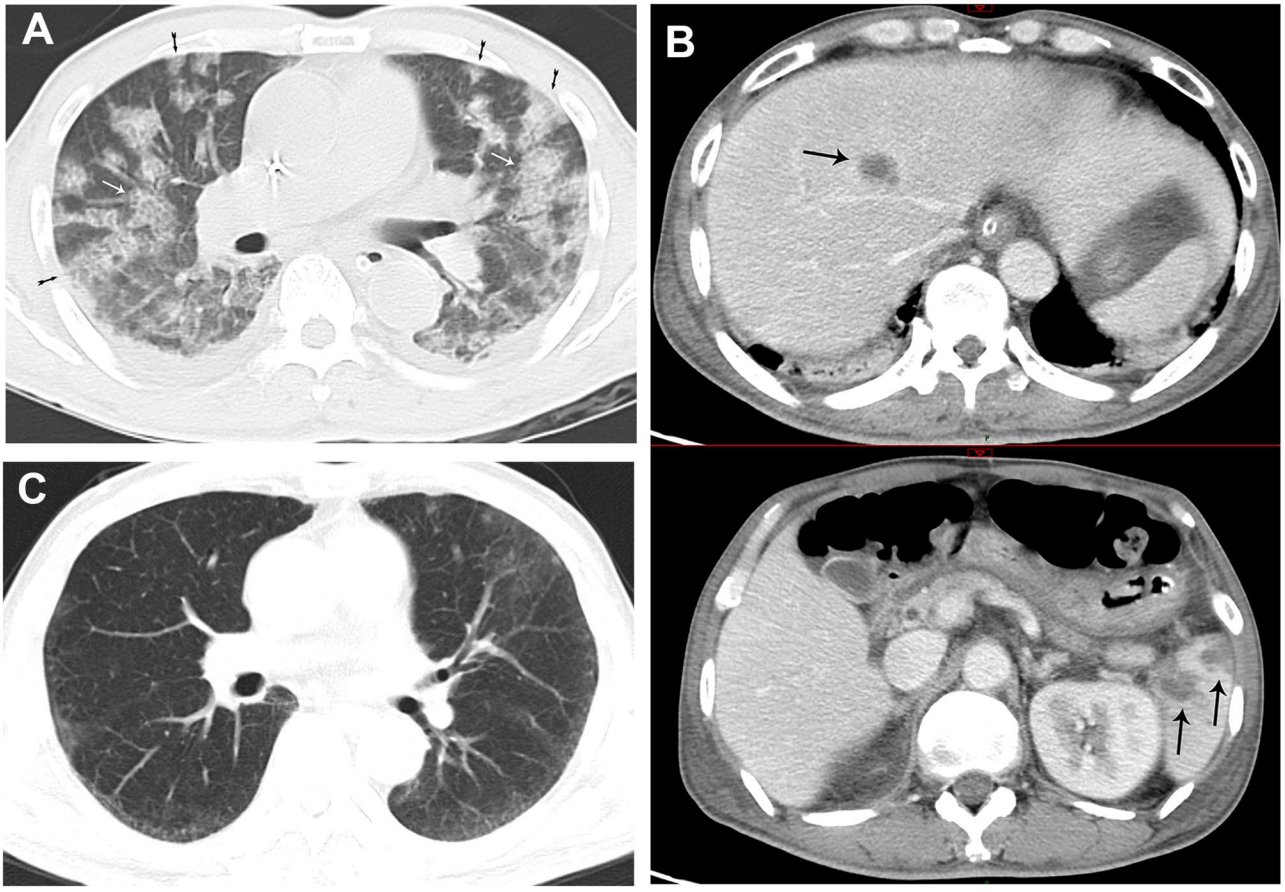

Fig. 4 Plain CT examination obtained in a man with positive blood culture for Burkholderia pseudomallei on admission. (**A**) Bilateral pulmonary and subpleural GGOs and ground glass nodules (fish tailed arrow), with "crazy-paving pattern"(white arrow) in GGO. (**B**) Enhanced CT showed multiple abscesses in the liver and spleen (arrow). (**C**) After 2 and a half months of follow-up, most of the lesions were absorbed and disappeared

is not specific, and bacterial culture is the gold standard for diagnosis, CT examination has the advantage of rapid diagnosis. Hematogenous infections can be indicated by lung manifestations and extrapulmonary lesions combined with lung abnormalities. Combining the history of living in epidemic areas with travel to epidemic areas and clinical indicators can prompt clinicians to respond quickly [34, 35].

Burkholderia pseudomallei, which has a high blood infection rate, is naturally resistant to a large number of antibiotics [2, 8, 36, 37] and requires longer bacterial culture times [2, 7, 37, 38]. New diagnostic methods, such as direct molecular testing from blood and Indirect immunofluorescence etc. have been developed, however, to date, none of them have sufficient sensitivity to replace culture assays, which is still the mainstay of laboratory diagnosis [2, 3, 8, 26, 39]. Therefore, in cases of clinical suspicion, employing complementary diagnostic methods other than laboratory tests may aid in the early diagnosis and management of the disease [1, 15, 20]. In situations where clinical sepsis persists and standard antibiotic treatments prove ineffective, if there is a delay in microbiological confirmation, both imaging and clinical signs can indicate to clinicians the possibility of a melioidosis infection in the bloodstream, then empirical therapy can enhance the overall treatment efficacy[1–3, 37, 40]. Imaging signs not only determine the location and extent of the lesion but can also serve as predictive indicators of disease outcomes and mortality [18].

Melioidosis is a tropical infectious disease that has been neglected for a long time [1, 2, 8, 26, 40], despite its high mortality rate and potential for prevention and treatment. Experts have pointed out that compared to many other tropical diseases that are considered neglected by the World Health Organization (WHO), the disease burden caused by melioidosis is greater [41]. This insight emphasizes the critical importance of prioritizing prevention and treatment efforts for melioidosis.

Limitations: Despite 20 years of data accumulation, the number of cases in this study was small and limited to

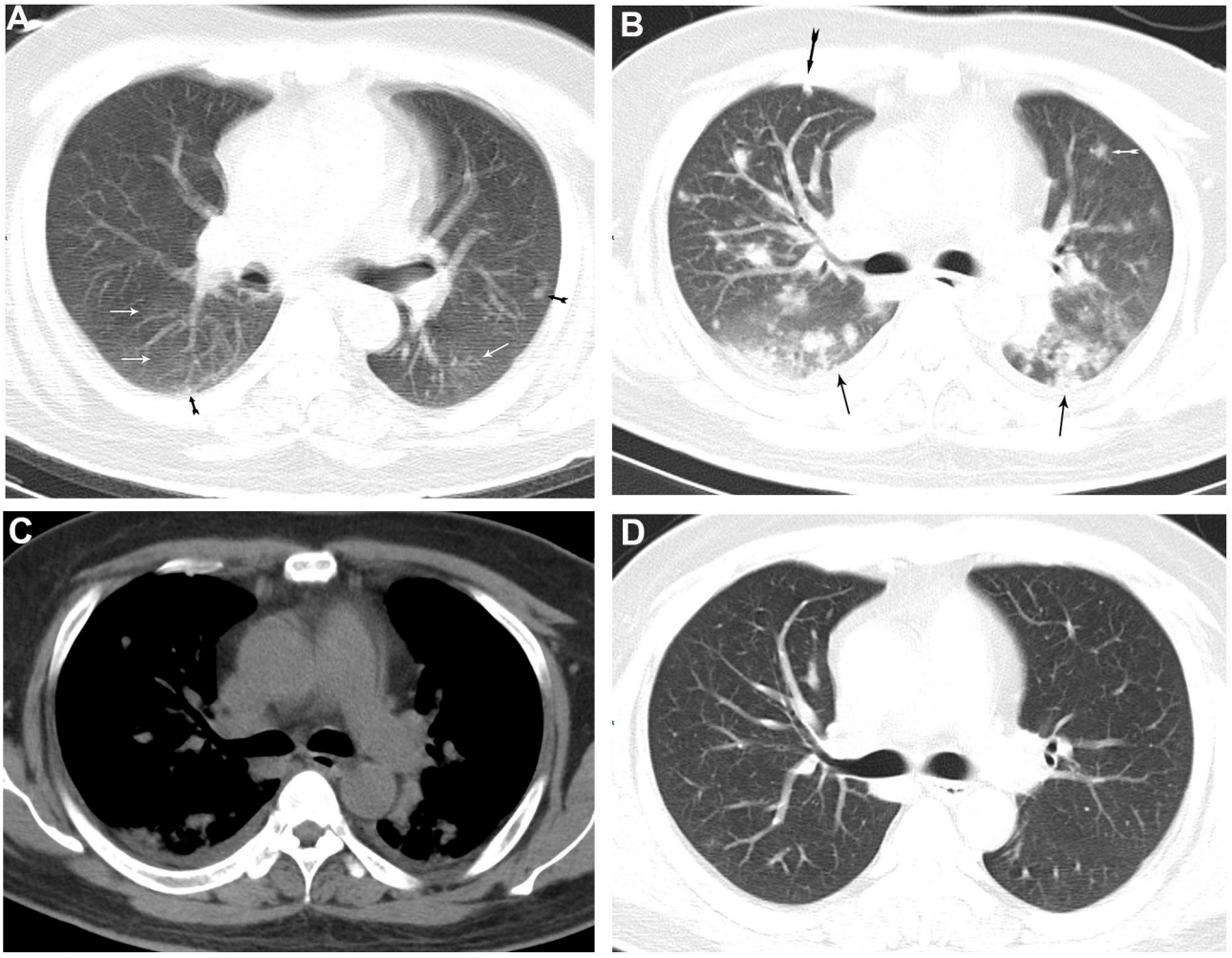

Fig. 5 Plain CT examination obtained in a man with positive blood culture for Burkholderia pseudomallei. Slice thickness of 5 mm. (**A**) GGO(white arrow) and nodules(fish tailed arrow) in both lungs. (**B**) After 3 days of follow-up, there was an increase in GGO and ground glass nodules in both lungs, and a small amount of pleural fluid, small nodules (fish tailed arrow) were visible. Subpleural micronodules could also be seen on both sides, with peribronchovascular interstitium thickening and GGO nearby (arrow). (**C**) Mediastinum window of (**B**). (**D**) After one month of treatment, reexamination showed that most of the GGO and nodules and subpleural micronodules in both lungs were absorbed, and bilateral pleural effusion was absorbed

Table 4 Logistic regression with clinical variables

B	S.E.	Wald	df	Sig.	Exp(B)	95% C.I.for EXP(B)		
						Lower	Upper	
Sex(1)	0.288	0.924	0.097	1	0.755	1.334	0.218	8.155
Age	−0.002	0.016	0.012	1	0.912	0.998	0.967	1.030
TemperatureGt39°C(1)	22.785	12000.264	0.000	1	0.998	7859133158.113	0.000	.
LeukocyteGt10(1)	−0.604	0.575	1.103	1	0.294	0.547	0.177	1.687
Diabetes(1)	1.446	0.516	7.852	1	0.005	4.247	1.544	11.678
Alcoholic(1)	1.286	0.849	2.293	1	0.130	3.618	0.685	19.119
Malignancy(1)	20.005	16685.498	0.000	1	0.999	487604794.677	0.000	.
Smoking(1)	−0.387	0.552	0.490	1	0.484	0.679	0.230	2.005
Constant	-22.015	12000.264	0.000	1	0.999	0.000		

Table 5 Logistic regression with clinical and radiologic variables

B	S.E.	Wald	df	Sig.	Exp(B)	95% C.I.for EXP(B)		
						Lower	Upper	
Sex(1)	−0.054	1.385	0.002	1	0.969	0.947	0.063	14.299
Age	−0.010	0.023	0.195	1	0.659	0.990	0.945	1.036
TemperatureGt39°C(1)	23.302	11256.079	0.000	1	0.998	13185497695.484	0.000	.
LeukocyteGt10(1)	-1.504	0.932	2.605	1	0.107	0.222	0.036	1.381
Diabetes(1)	1.834	0.791	5.380	1	0.020	6.262	1.329	29.507
Alcoholic(1)	2.346	1.836	1.633	1	0.201	10.444	0.286	381.556
Malignancy(1)	18.409	16877.531	0.000	1	0.999	98871633.140	0.000	.
Smoking(1)	−0.294	0.736	0.160	1	0.689	0.745	0.176	3.150
Nodule			7.793	2	0.020			
Nodule(1)	−0.530	1.188	0.199	1	0.655	0.589	0.057	6.036
Nodule(2)	2.235	0.866	6.659	1	0.010	9.349	1.712	51.066
Cavity			0.524	2	0.770			
Cavity(1)	−0.383	0.948	0.163	1	0.686	0.682	0.106	4.371
Cavity(2)	−0.779	1.161	0.450	1	0.502	0.459	0.047	4.463
Pneumonia			0.183	2	0.912			
Pneumonia(1)	−0.215	0.880	0.060	1	0.807	0.806	0.144	4.526
Pneumonia(2)	0.286	1.011	0.080	1	0.777	1.331	0.183	9.660
GGO			7.450	2	0.024			
GGO(1)	-1.754	1.225	2.049	1	0.152	0.173	0.016	1.911
GGO(2)	2.344	1.115	4.418	1	0.036	10.421	1.172	92.702
Hydrothorax			0.303	2	0.860			
Hydrothorax(1)	−0.575	1.107	0.270	1	0.603	0.563	0.064	4.924
Hydrothorax(2)	−0.348	1.054	0.109	1	0.742	0.706	0.090	5.574
Lymphadenopathy(1)	-1.342	0.961	1.949	1	0.163	0.261	0.040	1.720
CentrilobularNodules(1)	−0.687	0.837	0.674	1	0.412	0.503	0.098	2.593
ExtrapulmonaryLesions(1)	−0.052	0.789	0.004	1	0.947	0.949	0.202	4.456
Constant	-22.111	11256.079	0.000	1	0.998	0.000		

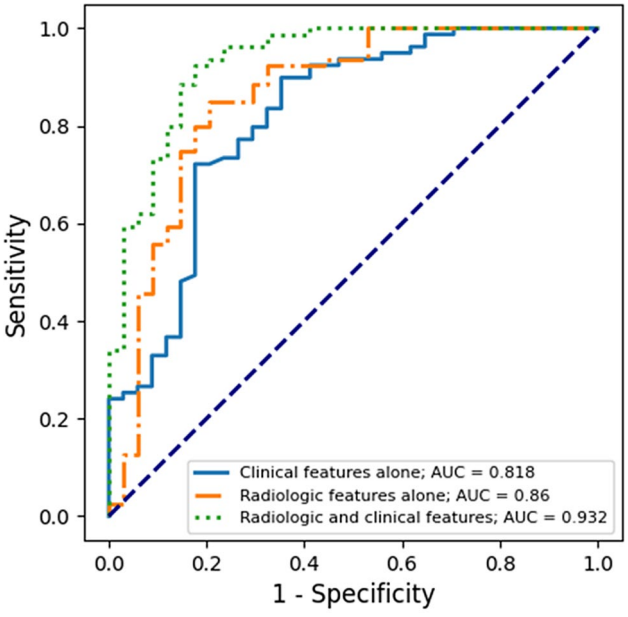

Fig. 6 Areas under the receiver operating characteristic curves

one hospital. This was a retrospective analysis, and there is a possibility of bias. The CT scan of the lung in this study is a traditional 5 mm thick slice used for the diagnosis of pulmonary infectious lesions, rather than lung tumor lesions. There is a difference in observing pulmonary GGO between 5 mm section and thin layer thickness. This article presents a comprehensive clinical and imaging investigation of hematogenous melioidosis, an infectious disease in tropical regions. However, the incidence of different pathogens and in different regions, as well as image features are still unclear and requires further observation.

In conclusion, the integration of imaging and clinical signs can serve as an early predictive tool for hematogenous infectious melioidosis, enabling timely intervention and treatment.

Table 6 Comparison between the clinical model and the model with clinical and radiologic features

Area under the curve						
Test result variable(s)	Area	Std. Error	Asymptotic Sig.*	Asymptotic 95% confidence interval		P-value†
				Lower Bound	Upper Bound	
Clinical features alone	0.818	0.046	0.000	0.727	0.909	0.012
Clinical and radiologic features	0.932	0.027	0.000	0.879	0.985	

Note * Null hypothesis: true area = 0.5

† Two-sided P-value obtained from DeLong test

Abbreviations

GGO Ground glass opacity
AUC Area under the receiver operating characteristic curve
ROC Receiver operating characteristic
ESM Electronic Supplementary Material

Supplementary Information

The online version contains supplementary material available at https://doi.org/10.1186/s12880-024-01471-6.

Supplementary Material 1

Acknowledgements
Not applicable.

Author contributions
Study concepts/study design: AL Y, LF S; data acquisition: XH L, F L，Q L，LF S; manuscript drafting: Q L, AL Y; article modification: Q L, DQ D, AL Y. Statistical analysis/article modification: SL T. All authors have approved the final version of submitted manuscript.

Funding
There was no Funding.

Data availability
All data supporting the conclusions of this article will be made available by the authors; further enquiries can be directed to the corresponding author.

Declarations

Ethics approval and consent to participate
This study was approved by the Ethics Committee of The First Affiliated Hospital of Hainan Medical University and the requirement for informed consent was waived. Our research was conducted in accordance with the Declaration of Helsinki.

Consent for publication
Not applicable.

Clinical trial number
Not applicable.

Competing interests
The authors declare no competing interests.

Received: 29 July 2024 / Accepted: 17 October 2024
Published online: 01 November 2024

References

1. Virk HS, Mukhopadhyay C, Wiersinga WJ, Melioidosis. A neglected cause of Community-Acquired Pneumonia. Semin Respir Crit Care Med. 2020;41:496–508.
2. Wiersinga WJ, Virk HS, Torres AG, et al. Melioidosis Nat Rev Dis Primers. 2018;4:17107.
3. Wiersinga WJ, Currie BJ, Peacock SJ, Melioidosis. N Engl J Med. 2012;13:367:1035–44.
4. White NJ. Melioidosis Lancet. 2003;361:1715–22.
5. Cheng AC, Currie BJ. Melioidosis: epidemiology, pathophysiology, and management. Clin Microbiol Rev. 2005;18:383–416.
6. Suputtamongkol Y, Chaowagul W, Chetchotisakd P, et al. Risk factors for melioidosis and bacteremic melioidosis. Clin Infect Dis. 1999;29:408–13.
7. Currie BJ, Mayo M, Ward LM, et al. The Darwin prospective melioidosis study: a 30-year prospective, observational investigation. Lancet Infect Dis. 2021;21:1737–46.
8. Samy RP, Stiles BG, Sethi G, Lim LHK. Melioidosis: clinical impact and public health threat in the tropics. PLoS Negl Trop Dis. 2017;11:e0004738.
9. Meumann EM, Cheng AC, Ward L, Currie BJ. Clinical features and epidemiology of melioidosis pneumonia: results from a 21-year study and review of the literature. Clin Infect Dis. 2012;54:362–9.
10. Mukhopadhyay A, Lee KH, Tambyah PA. Bacteraemic melioidosis pneumonia: impact on outcome, clinical and radiological features. J Infect. 2004;48:334–8.
11. Gassiep I, Armstrong M, Norton R. Human Melioidosis. Clin Microbiol Rev. 2020;33:e00006–19.
12. Alsaif HS, Venkatesh SK, Melioidosis. Spectrum of Radiological manifestations. Saudi J Med Med Sci. 2016;4:74–8.
13. Tan AP, Pui MH, Tan LK. Imaging patterns in melioidosis. Australas Radiol. 1995;39:260–4.
14. Yee KC, Lee MK, Chua CT, Puthucheary SD. Melioidosis, the great mimicker: a report of 10 cases from Malaysia. J Trop Med Hyg. 1988;91:249–54.
15. Tanphaichitra D. Acute septicaemic melioidosis with pulmonary hilar prominence: a case report with a unique chest radiographic pattern. Thorax. 1979;34:565–6.
16. Lim KS, Chong VH. Radiological manifestations of melioidosis. Clin Radiol. 2010;65:66–72.
17. Burivong W, Wu X, Saenkote W, Stern EJ. Thoracic radiologic manifestations of melioidosis. Curr Probl Diagn Radiol. 2012;41:199–209.
18. Khiangte HL, Vimala LR, Veeraraghavan B, Yesudhason BL, Karuppusami R. Can the imaging manifestations of melioidosis prognosticate the clinical outcome? A 6-year retrospective study. Insights Imaging. 2019;10:17.
19. Dhiensiri T, Puapairoj S, Susaengrat W. Pulmonary melioidosis: clinical-radiologic correlation in 183 cases in northeastern Thailand. Radiology. 1988;166:711–5.
20. Apisarnthanarak P, Thairatananon A, Muangsomboon K, Lu DSK, Mundy LM, Apisarnthanarak A. Computed tomography characteristics of hepatic and splenic abscesses associated with melioidosis: a 7-year study. J Med Imaging Radiat Oncol. 2011;55:176–82.
21. Ko JM, Park HJ, Kim CH. Pulmonary changes of pleural TB: up-to-date CT imaging. Chest. 2014;146:1604–11.
22. Silvestri GA, Gonzalez AV, Jantz MA, et al. Methods for staging non-small cell lung cancer: diagnosis and management of lung cancer, 3rd ed: American College of Chest Physicians evidence-based clinical practice guidelines. Chest. 2013;143(5 Suppl):eS211–S250.
23. DeLong ER, DeLong DM, Clarke-Pearson DL. Comparing the areas under two or more correlated receiver operating characteristic curves: a nonparametric approach. Biometrics. 1988;44:837–45.
24. roc_comparison. Available via https://github.com/yandexdataschool/ Accessed 16 Feb 2024.
25. Lee JY, Lee KS, Jung KJ, et al. Pulmonary tuberculosis: CT and pathologic correlation. J Comput Assist Tomogr. 2000;24:691–8.
26. Meumann EM, Limmathurotsakul D, Dunachie SJ, Wiersinga WJ, Currie BJ. Burkholderia pseudomallei and melioidosis. Nat Rev Microbiol. 2024;22:155–69.
27. McGuinness G, Naidich DP, Jagirdar J, Leitman B, McCauley DI. High resolution CT findings in miliary lung disease. J Comput Assist Tomogr. 1992;16:384–90.

28. Hong SH, Im JG, Lee JS, Song JW, Lee HJ, Yeon KM. High resolution CT findings of miliary tuberculosis. J Comput Assist Tomogr. 1998;22:220–4.
29. Oh YW, Kim YH, Lee NJ, et al. High-resolution CT appearance of miliary tuberculosis. J Comput Assist Tomogr. 1994;18:862–6.
30. Yu An-le. Chen Hai, Li Qun. Analysis of melioidosis of 12 cases on imaging and clinic. Chin J Radiol. 2007;41:1186–8.
31. Collins J. CT signs and patterns of lung disease. Radiol Clin North Am. 2001;39:1115–35.
32. Karaosmanoglu AD, Uysal A, Onder O, et al. Cross-sectional imaging findings of splenic infections: is differential diagnosis possible? Abdom Radiol (NY). 2021;46:4828–52.
33. Perez AR, Aburayyan N, Domingo MRS Jr, Onglao M. Disseminated melioidosis presenting as pneumonia, femoral and sacral osteomyelitis, splenic abscess and high rectal fistula: a case report and review of literature. Int J Surg Case Rep. 2021;89:106588.
34. Chong VF, Fan YF. The radiology of melioidosis. Australas Radiol. 1996;40:244–9.
35. Muttarak M, Peh WCG, Euathrongchit J, et al. Spectrum of imaging findings in melioidosis. Br J Radiol. 2009;82:514–21.
36. Bugrysheva JV, Sue D, Gee JE, et al. Antibiotic Resistance Markers in Burkholderia pseudomallei strain Bp1651 identified by genome sequence analysis. Antimicrob Agents Chemother. 2017;61:e00010–17.
37. Stephens DP, Thomas JH, Ward LM, Currie BJ. Melioidosis causing critical illness: a review of 24 years of experience from the Royal Darwin Hospital ICU. Crit Care Med. 2016;44:1500–5.
38. Chakravorty A, Heath C, Melioidosis. An updated review. Aust J Gen Pract. 2019;48:327–32.
39. Currie BJ. Melioidosis and Burkholderia pseudomallei: progress in epidemiology, diagnosis, treatment and vaccination. Curr Opin Infect Dis. 2022;35:517–23.
40. Khiangte HL, Vimala LR, Eapen A, Veeraraghavan B, Karuppusami R, Gibikote S. A retrospective case-control study to evaluate the Diagnostic Accuracy of Honeycomb Sign in Melioid Liver Abscess. Am J Trop Med Hyg. 2018;99:852–7.
41. Birnie E, Virk HS, Savelkoel J, et al. Global burden of melioidosis in 2015: a systematic review and data synthesis. Lancet Infect Dis. 2019;19:892–902.

Publisher's note